Compact Installation for Testing Vectored-Thrust Engines

W. H. Cunningham* and J. F. Boytos†
Naval Air Propulsion Center, Trenton, New Jersey

An installation has been built to test the Pegasus engine in its vectored-thrust mode, in a conventional enclosed sea-level test cell, in response to the Navy's requirement for test facilities for V/STOL propulsion systems. The main features of the installation are the hardware for measuring vectored thrust and for redirecting engine exhaust gases out of the cell. This was accomplished by a cascade of turning vanes installed in exhaust collector ducts downstream of each engine nozzle. The design of the four cascades has some unique characteristics. The major criteria for the installation were met; effects on engine performance were minimal, and engine steady-state and transient operation was satisfactory from idle to maximum power. The overall performance of cascade turning vanes operating at high subsonic Mach numbers and high Reynolds numbers was also investigated.

Nomenclature

c	= constant
d	= differential
F	= thrust
f	= function to be defined
h	= width of subinterval of integration
M	= Mach number
N	= revolutions per minute (rpm)
p	= pressure
R	= radius, or reaction
s	= path length
T	= temperature
V	= velocity
W	= weight
α	= nozzle angle
Γ	= circulation = $\oint V \cdot ds$
γ	= ratio of specific heats
θ	= temperature correction
ρ	= density

Subscripts (and Superscript)

a,b	= stations or limits of integration
B	= bellmouth
H	= horizontal
L	= engine low-pressure spool (fan)
$0,i,k$	= numerical integration or subinterval indices
t	= total or stagnation conditions
V	= vertical
$( )^*$	= sonic flow
∞	= freestream or uniform flow

Introduction

SINCE the introduction of the Harrier V/STOL aircraft into service with the United States Marine Corps, the Navy has been concerned with providing facilities to test the unique power plant of this aircraft—the Pegasus vectored-thrust turbofan engine. The Naval Air Propulsion Center (NAPC) recently modified an existing altitude and a sea-level test cell, overcoming a number of technical challenges, to provide the capability to test this high mass flow engine.

The Rolls-Royce Pegasus vectored-thrust turbofan engine, designated the F402-RR-402, is a simple type of V/STOL power plant. It is basically a conventional turbofan engine which, by the addition of a simple swiveling nozzle system, provides vertical thrust for takeoff and landing and horizontal thrust for conventional flight. The engine is shown schematically in Fig. 1.

To test a large vectored-thrust engine, such as the F402, in an enclosed ground test facility, the following requirements were established:

1) Thrust measurements were required in the horizontal, vertical, and transitional modes.

2) No engine exhaust gas recirculation into the test cell area was permitted.

3) The exhaust gas collectors could not impose any adverse effects on engine performance.

4) The engine had to be mounted on the centerline of the test cell to permit plant conditioned air to be supplied to the engine, if desired.

This article describes the analytical work, design, scale model, and full-scale engine test efforts accomplished by NAPC to develop the capability to test the Pegasus vectored-thrust engine.

Installation Overview

A sketch of the engine installation (top view) with the four exhaust gas collector ducts is shown in Fig. 2 for a sea-level test cell. In a conventional cell, the exhaust stack is located directly behind the engine test stand, but when the Pegasus engine is mounted for testing, its exhaust nozzles are pointed at either the rear walls or the floor. A project to test thrust reversers in an engine cell would be faced with exactly the same problem. For this reason, some ducts are necessary to reposition and redirect the exhaust streams, and they have some severe design requirements. The exhaust properties include Mach numbers close to 1.0, dynamic pressures up to 15 psi, and temperatures up to 250°F for the cold nozzles and 1250°F for the hot nozzles. Space constraints require exhaust turning angles of up to 120 deg, depending on the nozzle angle. The momentum of the exhaust gases has to be retained as much as possible to avoid having to pump the gases out of the cell. A side-view cutaway emphasizing the front and rear collector ducts with vane cascades installed is shown in Fig. 3.

A diagram of the thrust measuring system is shown in Fig. 4, with the location of forces acting on the system. The test stand supporting the engine is bolted to a thrust bed, which in turn is suspended at the corners. For horizontal thrust measurement, the bed pushes against a load cell. For the vertical component, there is a load cell in each of the four corner suspensions, and the bed is weighted to always keep the load cells in tension.

Presented as Paper 81-1592 at the AIAA/SAE/ASME 17th Joint Propulsion Conference, Colorado Springs, Colo., July 27-29, 1981; submitted Sept. 4, 1981; revision received May 4, 1982. This paper is declared a work of the U.S. Government and therefore is in the public domain.

*Installation Design Engineer.
†Program Manager.

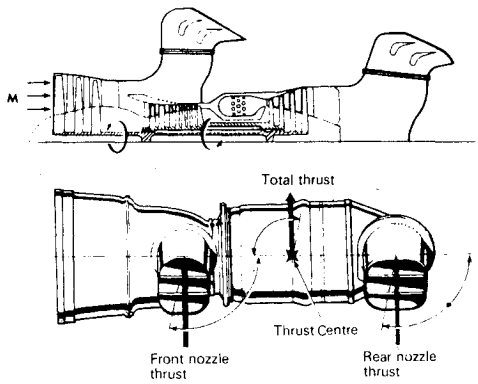

Fig. 1 The vectored-thrust power plant.

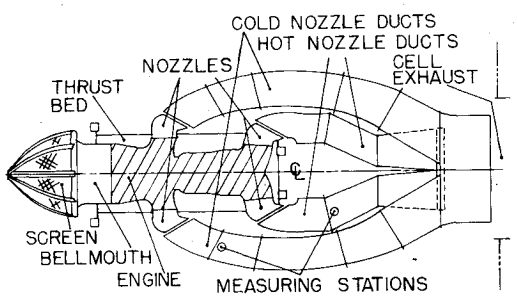

Fig. 2 Top view of engine and collector ducts installation in sea-level cell.

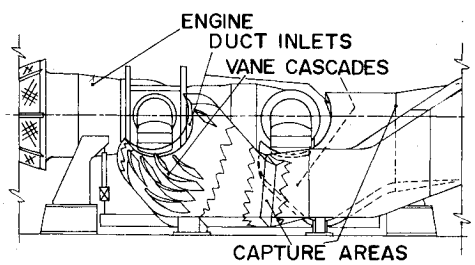

Fig. 3 Collector duct configuration.

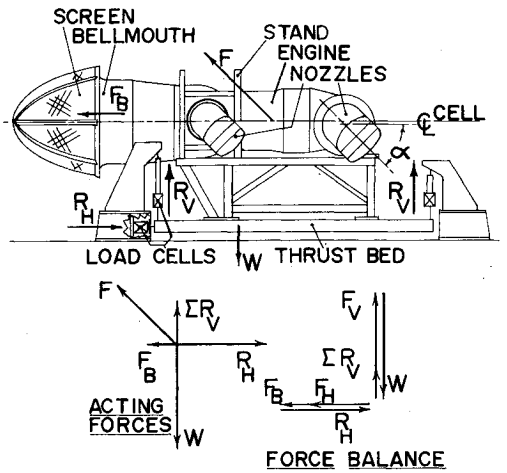

Fig. 4 Engine thrust measurement.

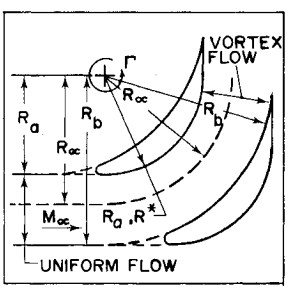

Fig. 5 Vane flow model.

The force balances are also shown in Fig. 4. The weight W is the sum of the vertical load cell readings with the engine at rest. With the engine running, the load cells read one horizontal and four vertical reactions, R_H and R_V. The bellmouth correction F_B is calculated from pressure measurements, and the engine thrust components, F_H and F_V, from the force balances.

Theoretical Analysis: Vane Cascade Design

Collector ducts were used to direct the engine exhaust flows out of the test cell. In order for the collector ducts to function effectively with the engine nozzles in either the horizontal or vertical configurations, vane cascades were designed for use in the ducts.

To turn the engine exhaust gases, circular-arc thick-vane cascades[1] were selected because of their relative compactness and efficiency. The vane spacing was critical, however, because the vanes were required to turn the high-velocity compressible flow through large angles. The spacing was defined in terms of the ratio of the radius of the concave surfaces of the vanes to that of the convex surfaces. The radius ratio was calculated using a compressible vortex as a flow model. This approach is believed to be unique for the problem of cascade design. It provided good results even though secondary flows and boundary layers, which strongly affect the actual operation, were not evaluated in this analysis.

The approach assumed that 1) the two-dimensional vortex had the same stagnation pressure as the incoming uniform flow to the vanes, and 2) its center is the center for the radii for the passage between adjacent vanes. This is illustrated in Fig. 5. The reasoning behind this vane design approach is as follows:

1) There is a circular flow path in the vortex for which the flow properties are the same as those of the uniform flow. The properties of interest are static pressure, static temperature, and Mach number. The radius of the circle is called the isobaric radius R_∞ because of the static pressure identity.

2) The inner radius of the vane passage, R_a, which is also the convex radius of the vane, is the radius of the circle in the vortex whose Mach number is as close to 1.0 as practical, so that shocks do not form at the convex surface.

3) The outer radius, R_b, of the passage (concave radius of the vane) is the radius for which the flow in the passage is the same as the uniform flow through a flow area with a width equal to the difference between the convex and concave radii. This flow area is unique because the flow through identical differential areas will not be the same for uniform flow and compressible flow in a vortex.

The outer and inner radii are expressed as radius ratios to the isobaric radius and therefore can be scaled up and down; this is possible under conditions using a compressible, inviscid fluid. For information, the real-fluid effects during testing were significant but not prohibitive as far as the design was concerned.

The properties in the vortex can be found by considering the Bernoulli equation, the vortex flow equation, and the equation for an isentropic process. The Bernoulli equation in differential form is

$$\frac{dp}{\rho} = -V\,dV$$

For this vortex, $VR = \Gamma/2\pi = V_\infty R_\infty$. The freestream properties are held constant. Then

$$V = V_\infty R_\infty / R \quad \text{and} \quad dV = -(V_\infty R_\infty / R^2)\,dR$$

In an isentropic process, $p/\rho^{\gamma} = \text{const} = p_{\infty}/\rho_{\infty}^{\gamma}$; therefore $1/\rho = (1/\rho_{\infty})(p_{\infty}/p)^{1/\gamma}$. Substituting back into the Bernoulli equation and using $\rho V^2 = \gamma p M^2$,

$$p_{\infty}^{1/\gamma}\frac{dp}{p^{1/\gamma}} = -\rho_{\infty}\left(\frac{V_{\infty}R_{\infty}}{R}\right)\left(-\frac{V_{\infty}R_{\infty}}{R^2}dR\right)$$

$$= \rho_{\infty}V_{\infty}^2R_{\infty}^2\frac{dR}{R^3} = \gamma p_{\infty}M_{\infty}^2R_{\infty}^2\frac{dR}{R^3} \tag{1}$$

Finally,

$$\frac{1}{p_{\infty}^{(\gamma-1)/\gamma}}\int\frac{dp}{p^{1/\gamma}} = \gamma M_{\infty}^2R_{\infty}^2\int\frac{dR}{R^3} \tag{2}$$

Integrating,

$$\frac{\gamma}{\gamma-1}\left(\frac{p}{p_{\infty}}\right)^{(\gamma-1)/\gamma} = -\frac{\gamma M_{\infty}^2}{2}\left(\frac{R_{\infty}}{R}\right)^2 + C$$

For $p = p_{\infty}$ and $R = R_{\infty}$,

$$1 + \frac{\gamma-1}{2}M_{\infty}^2 = \frac{\gamma-1}{\gamma}C$$

The result is

$$\left(\frac{p}{p_{\infty}}\right)^{(\gamma-1)/\gamma} = 1 + \frac{\gamma-1}{2}M_{\infty}^2 - \frac{\gamma-1}{2}M_{\infty}^2\left(\frac{R_{\infty}}{R}\right)^2 \tag{3}$$

Substituting the relationship

$$\left(\frac{p}{p_{\infty}}\right)^{(\gamma-1)/\gamma} = \frac{T}{T_{\infty}} = \frac{1+[(\gamma-1)/2]M_{\infty}^2}{1+[(\gamma-1)/2]M^2}$$

into Eq. (3) and solving for the radius ratio yields

$$\left(\frac{R_{\infty}}{R}\right)^2 = \left(\frac{M}{M_{\infty}}\right)^2\left(\frac{1+[(\gamma-1)/2]M_{\infty}^2}{1+[(\gamma-1)/2]M^2}\right)$$

or

$$\frac{R_{\infty}}{R} = \frac{M}{M_{\infty}}\sqrt{\frac{T}{T_{\infty}}} \tag{4}$$

Setting $M = 1.0$, $R = R^*$, and inverting, for local sonic conditions,

$$\frac{R^*}{R_{\infty}} = M_{\infty}\Big/\sqrt{\frac{2}{\gamma+1}\left(1+\frac{\gamma-1}{2}M_{\infty}^2\right)} \tag{5}$$

It is possible for Mach numbers greater than 1.0 to exist locally without forming shocks.[2] A shock would not tend to propagate laterally because the flow becomes subsonic as the radius increases. The minimum practical convex surface radius therefore may be slightly smaller than Eq. (5) would predict, and Eq. (4) would be used with a slightly larger Mach number. In using the results of this investigation, the convex radius R_a was taken as R^* for the M_{∞} selected for the cascade design. In addition, Eq. (3) can be used to determine ideal flow properties in existing turning vane cascades in order to investigate departures.

The concave radius R_b can be found by comparing the flow in a given vane passage to the corresponding uniform flow. The flow area is adjusted until the two mass flows are equal with the depth of the uniform flow equal to the difference in vane passage radii. Thus

$$\int_{R_a}^{R_b}(\text{vortex mass flow})\,dR = \int_{R_a}^{R_b}(\text{uniform mass flow})\,dR \tag{6}$$

In the uniform flow, the location of R_a is arbitrary.

This approach works because compressible flows through equal flow areas are not equal under different flow conditions. More precisely, the comparison of flows through differential areas, one a compressible vortex and the other a compressible uniform flow, reduces to a comparison of the flow functions and shows that they are equal only if the Mach numbers are equal. From Ref. 2,

$$\frac{\rho V dA}{\rho_{\infty}V_{\infty}dA} = \frac{M}{M_{\infty}}\left(\frac{1+[(\gamma-1)/2]M_{\infty}^2}{1+[(\gamma-1)/2]M^2}\right)^{(\gamma+1)/2(\gamma-1)}$$

$$> 1 \text{ for } M > M_{\infty}$$

$$< 1 \text{ for } M < M_{\infty} \tag{7}$$

When the integration is performed, the cumulative vortex flow increases faster than the uniform flow until the isobaric radius is reached. It then increases more slowly until the cumulative uniform flow catches up. The following equations are used to evaluate the flow that exhibits the above characteristics. The algebra for Eq. (6) is

$$\int_{R_a}^{R_b}\rho V dR = \rho_{\infty}V_{\infty}\int_{R_a}^{R_b}dR \tag{8}$$

$$\int_{R_a}^{R_b}\rho\frac{\Gamma}{2\pi R}dR = \rho_{\infty}\frac{\Gamma}{2\pi R_{\infty}}\int_{R_a}^{R_b}dR$$

$$\int_{R_a}^{R_b}\frac{\rho}{\rho_{\infty}}\frac{dR}{R} = \frac{1}{R_{\infty}}\int_{R_a}^{R_b}dR = \frac{R_b}{R_{\infty}} - \frac{R_a}{R_{\infty}} \tag{9}$$

From the flow properties relationship, Eq. (3),

$$\left(\frac{p}{p_{\infty}}\right)^{1/\gamma} = \frac{\rho}{\rho_{\infty}} = \left[1+\frac{\gamma-1}{2}M_{\infty}^2 - \frac{\gamma-1}{2}M_{\infty}^2\left(\frac{R_{\infty}}{R}\right)^2\right]^{1/(\gamma-1)}$$

Then

$$\int_{R_a}^{R_b}\left[1+\frac{\gamma-1}{2}M_{\infty}^2 - \frac{\gamma-1}{2}M_{\infty}^2\left(\frac{R_{\infty}}{R}\right)^2\right]^{1/(\gamma-1)}\frac{dR}{R}$$

$$= \frac{R_b}{R_{\infty}} - \frac{R_a}{R_{\infty}} \tag{10}$$

There is no convenient integral for the left side of Eq. (10). For this project it was evaluated numerically using Simpson's one-third rule.[3] The equation is

$$\int_a^b f(x)\,dx \cong (h/3)(f_0 + 4f_1 + 2f_2 + 4f_3 + 2f_4 + \ldots 4f_{n-1} + f_n) \tag{11}$$

where the interval (a,b) is divided into n equal subintervals. The error term at the end of the equation is not shown. For this application,

$$f_i = f(R_i) = \frac{1}{R_i}\left[1+\frac{\gamma-1}{2}M_{\infty}^2 - \frac{\gamma-1}{2}M_{\infty}^2\left(\frac{R_{\infty}}{R_i}\right)^2\right]^{1/(\gamma-1)} \tag{12}$$

In addition,

$$\int_{R_k}^{R_{k+2}}f(R)\,dR = \int_{R_0}^{R_k}f(R)\,dR + (h/3)(f_k + 4f_{k+1} + f_{k+2}) \tag{13}$$

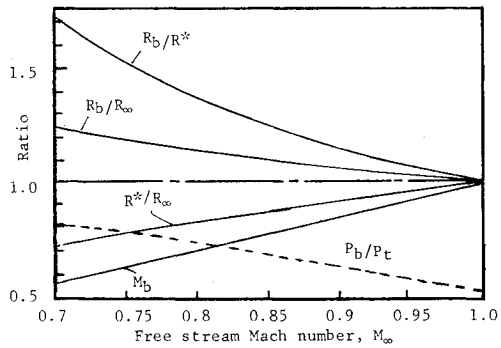

Fig. 6 Vane flow properties.

which allows R_b in Eq. (10) to be increased successively on both sides of the equation until it balances. This was the method used to find R_b, whereupon the ideal flow properties at the concave vane surface could be calculated. Figure 6 shows the values of the convex radius R^* and the concave radius R_b expressed as ratios to the isobaric radius R_∞. The overall radius ratio R_b/R^*, the Mach number M_b, and the static-to-total-pressure ratio P_b/P_t at the concave vane surface are also shown as a function of freestream Mach number.

Experimental Investigations: Scale Model Nozzle/Vane Cascade Tests

Even with the results of the theory, there were many questions to be answered concerning the design, so a test program was conducted using a one-quarter-scale, cold gas model. The areas explored were as follows:

1) The practicality of designing a cascade with a radius ratio dictated by the theory had to be verified. Theory indicated that building vanes for Mach numbers close to 1.0 would require many thin, closely spaced vanes, too impractical to fabricate and operate under engine test conditions. A more practical cascade would have to operate in flows with M_∞ higher than that for which it was designed.

2) Entrance effects and the effects of secondary flow, separation, boundary layer, and vane angle of attack had to be addressed. Vane angle of attack is especially significant in the design because it can vary with nozzle position by as much as 30 deg, whereas cascades are normally designed assuming that the direction of the incoming flow is fixed. Only part of the cascade is in the engine flow at any one time, unlike usual cascade designs.

3) The flow properties downstream of the cascade had to be determined. For example, was there enough energy to move the exhaust gases completely out of the cell or was additional pumping required? There was also the problem of exhaust gas recirculation; if the gases are allowed to recirculate into the test cell, they can heat it excessively or be reingested into the engine.

The one-quarter-scale model is shown in Fig. 7. The following lists some of its features:

1) A vane cascade turned the air back to the horizontal from a nozzle angle of from 30 deg (down) to 105 deg (or just forward of the vertical). The vanes had a 5-in. span, chords of 5 in., and convex and concave radii that varied from a minimum of 2.75 to a maximum of 5.03 in., with a convex to concave radius ratio of 1.3, which corresponds to a freestream Mach number of slightly less than 0.85. A single row of vanes, machined from steel pipe sections, was used. Static pressure taps were machined into the convex and concave surfaces to gather data to support the theory. A set of three vanes that had convex surfaces extending all the way to the trailing edges was also tested. Full-scale vanes were much easier to make with this geometry than conventional SAE thick vanes.[1]

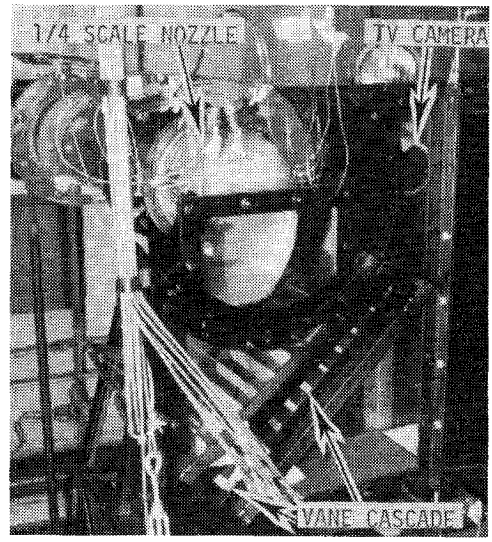

Fig. 7 Nozzle/cascade scale model.

2) A fan exhaust nozzle (front nozzle as shown in Fig. 1) of the Pegasus engine with two aluminum vanes inside was reproduced to one-quarter scale from molded fiberglass. The top vane had three total pressure taps and two thermocouples in the leading edge and two static taps each in the concave and convex surfaces. The inlet had a collar that was held to the air supply duct with a V-band clamp, which allowed the nozzle to be positioned at any desired nozzle angle.

3) The area downstream of the cascade had one side of clear plastic and the other painted white. Tufts were strung on rods spaced equally through the area so the flows could be videotaped during testing. The "tufts" were made of wire because of the high flow velocities. There were two plates at the back of the model that could be adjusted to simulate long ducts with turns behind the cascades.

The model test results follow:

1) The cascade, designed according to theory, turned the flow through all nozzle angles with sufficient energy to exhaust it from the test cell. Increasing the vane spacing by 30% degraded the flow properties significantly; in fact, with the spacing doubled, most of the momentum and energy in the flow was lost, although the flow was still turned. In particular, flow separation was evident through the entire vane passage, because the convex pressures were near ambient and the concave pressures were very high. Thus all of the pressure to turn the flow was provided by the concave surface of the vane, which acted as a scoop or shovel rather than as a vane. The spacing then determined the mass flow through the passage and the pressure at the concave surface required to turn it. Changing the spacing and using the same vanes also altered the geometry of the passages, causing some of the losses in flow properties.

2) Testing was conducted at angles of attack on the instrumented vanes from -15 to $+15$ deg, with the angle of attack taken from a straight line tangent to the camber line of the vane at the leading edge, rather than from the chord line. At large positive angles of attack, flow separation at the leading edges was evident, but it appeared to reattach at or in front of the 30% chord position on the convex surface, at freestream Mach numbers up to 0.96. At small angles, vane flow predominated throughout the engine power range tested. In general, the cascade was very tolerant to changes in angle of attack.

3) The tuft behavior showed considerable recirculation with the cascade exhausting horizontally; however, when the flow area behind the cascade and the nozzle was made smaller, recirculation was reduced to reasonable levels. In the full-scale design, therefore, the flow from the cascade converges

to a capture area, rather than exiting in a uniform direction—another departure from conventional cascade design.

4) The static pressure measurements at the vane surfaces were comparable to those predicted by theory. In addition, the distributions were nearly constant through the vane passages, indicating approximately uniform turning forces, which would be expected with circular-arc vanes. The flow separations at off-design conditions were also clearly indicated.

Fabrication of Full-Scale Vane Cascades

Construction of the full-scale vane cascades was based on the results of the scale model tests. The one-quarter-scale model used a single row of vanes in its cascade, the locations of which were determined from the nozzle velocity vectors and the desired direction of the flow leaving the cascade. In the layout of the full-scale design; it was found that one row of vanes would not fit between the desired engine nozzle positions and the floor of the cell. To accommodate these space restrictions, the design was reworked into the compound pattern shown in Fig. 8. In addition, it was found that the orientation of the cascades allowed much of the redirection of the air toward or away from the engine centerline to be accomplished by the vanes as well. The vanes were made as large as practical for strength in the hot exhaust, and to reduce the number required and the fabrication costs. Construction of the full-scale vanes is illustrated in Fig. 9.

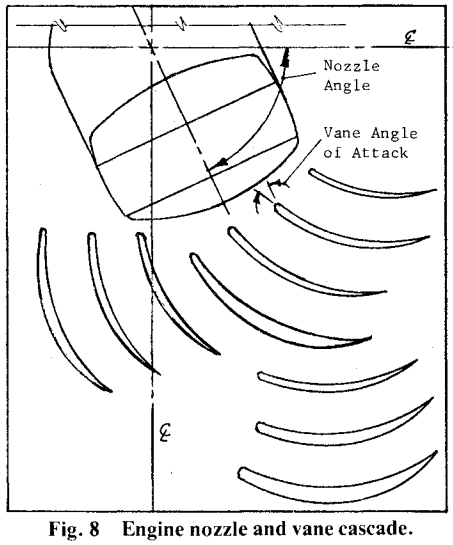

Fig. 8 Engine nozzle and vane cascade.

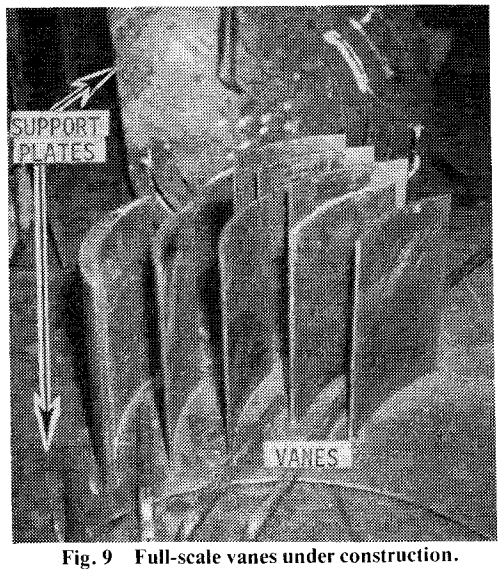

Fig. 9 Full-scale vanes under construction.

Exhaust Gas Collector Ductwork

In front of the cascades were the duct inlets. The engine nozzles exhausted into the collector ducts through these openings, which were large enough to allow the nozzles to be set at any required angle. The unused areas of the inlets were covered with steel plates to prevent recirculation of exhaust gases back into the test cell. Because of this arrangement, however, the nozzles could not be moved while the engine was running, even though they could when the engine is installed in the aircraft.

The rest of the ductwork consisted of capture areas behind the vanes and various turns to get the air back to the centerline of the cell and into the cell exhaust duct. The capture areas were made as small as possible without back pressuring the flow (the model tests had shown that larger capture areas would increase recirculation). Downstream of the capture areas, the duct flow areas were increased gradually in the turns to minimize back pressure on the flow. The concern was that the back pressure would tend to force exhaust out through the duct nozzle openings, around the engine and into the cell, cause cell overheating, engine hot air ingestion, and associated performance and instrumentation problems. Later, tests showed that the downstream ducts did act as diffusers, as the area static pressures were 3-6 in. Hg below cell ambients at high power. In addition, when the nozzle inlets were opened wide during the latter part of the testing, there was no evidence of recirculation.

The cold nozzle ductwork was fabricated from mild steel, and the hot nozzle ducts from AISI Type 304 stainless steel. The thin vanes were machined from rolled steel plates; the thick ones were of steel sheet welded over a framework. All of the vanes had a convex radius of 20 in. and a concave radius of 26 in. Both the hot and cold nozzle ducts on the left side of the engine were instrumented. Total pressure taps were built into the leading edges of some of the vanes.

The ducts were welded from ¼-in.-thick plates and stiffened externally. Static pressure taps were placed in the duct walls at locations of interest during construction. The hot nozzle ducts and the rear portions of the cold nozzle ducts were insulated to minimize heat rejection to the cell. The size and orientation of the exhaust collector ducting installed in the sea-level test cell is shown in Fig. 10.

Engine Tests: V/STOL Engine Used as Test Vehicle

To test the full-scale exhaust collector ducts with vane cascades, the equipment was installed in an NAPC sea-level test cell and connected to an F402-RR-402 engine.

The F402-RR-402 is a vectored-thrust turbofan engine with a nominal bypass ratio of 1.4. It has three low-pressure

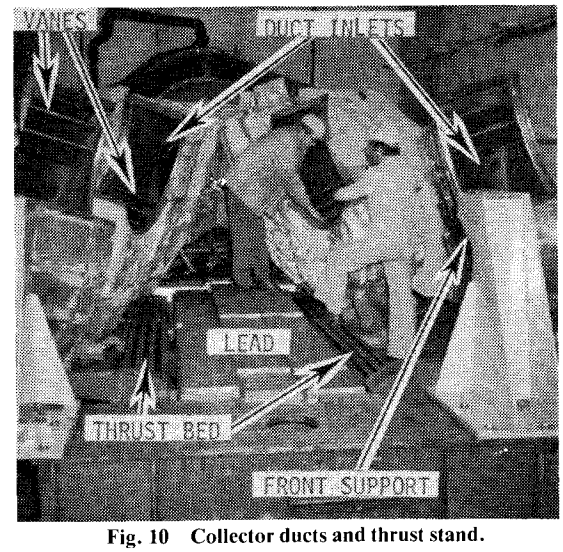

Fig. 10 Collector ducts and thrust stand.

compressor stages on one spool, and eight high-pressure compressor stages on a second spool, each spool being independently driven by separate two-stage turbines through contrarotating coaxial shafts. The inlet to the high-pressure spool is controlled by variable inlet guide vanes. All lifting and propulsive thrust is delivered by four symmetrically positioned vectoring-thrust nozzles, two at the front of the engine discharging a proportion of the low-pressure compressor air, and two at the rear discharging all the turbine gases. The combustion chamber is of the annular vaporizing type. Thrust augmentation is provided by an engine water injection system.

The engine is capable of providing a large air bleed from the high-pressure compressor outlet for aircraft stabilization and control purposes. The fuel pumps and hydromechanical fuel control unit, together with a jet pipe temperature limiter (JPTL), provide control of fan speed and engine transient and steady-state operation.

Thrust System

For engine thrust measurements, the test stand that supports the engine is bolted to a thrust bed, which in turn is suspended at the corners. For horizontal measurement, the thrust bed pushes against a load cell. For the vertical components, four load cells are built into the four corner suspensions (one each). The bed is weighted to keep the cells always in tension, and the vertical thrust components are determined from the difference between loads measured with the engine running and at rest, as has been noted in Fig. 4.

Operational Results

Facility operational capabilities were verified using the F402 engine as the test vehicle, since it is the only V/STOL engine available in the Navy inventory. Engine and facility operation were satisfactory while running with engine nozzles in the horizontal, vertical, and slant mode directions. Engine thrust was successfully measured for all configurations tested, based upon a comparison against steady-state and transient data previously acquired with the engine. Thrust measurement accuracy was $\pm 1\%$ for either horizontal or vertical axes, and within $\pm 3\%$ for the slant mode configuration (engine nozzles between 0 and 90 deg). Additional refinements to the installation are planned to improve the measurement of thrust in the slant mode.

Collector Duct Performance

Facility installation performance was evaluated from the standpoint of comparisons of data from these tests with other Pegasus engine test data, thrust measurement suitability, and vane cascade efficiency. The method for this last evaluation was similar to that used to measure the performance of a jet pump, where a measuring station was established downstream of the cascade, and conditions upstream of the cascade were determined from properties of engine and cell ambient airflows. Variations in mass flow, momentum, and kinetic energy plus flow work, at various engine powers and nozzle angles, were used as criteria. Figures 11 and 12 are from data plots generated during testing.

There were two measuring stations, both behind the left side of the engine, one in each nozzle duct. Each station consisted of a rake for measuring temperature and total pressure distributions, and pressure taps in the duct walls for measuring static pressure. At the top and bottom of the stations, pitot tubes were installed facing downstream to check for recirculation. Also installed were static pressure taps in the duct walls in the cascades and total pressure taps in the leading edges of some of the vanes. The total pressure taps in the rakes were designed to read the full value of the total pressure in spite of large variations in the direction of the flow at the rakes. This was necessary because the cascades exhausted the flows into the capture areas from different

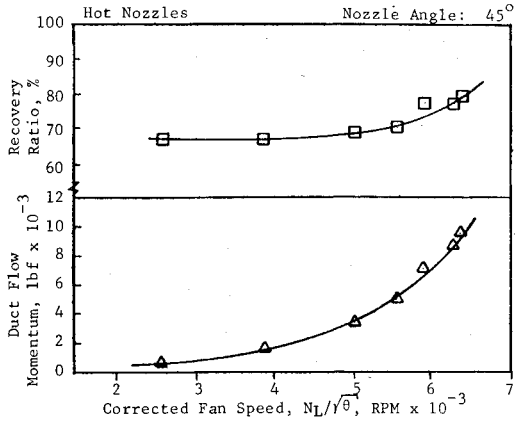

Fig. 11 Collector duct performance (momentum flux).

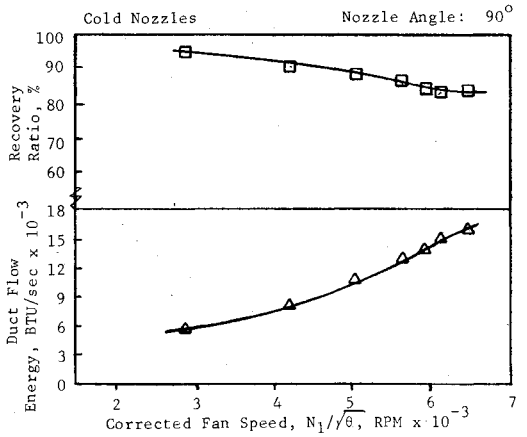

Fig. 12 Collector duct performance (energy flux).

angles, depending on the direction of the incoming flows from the nozzles. Nozzle angles from horizontal to 105 deg down produced corresponding flows into the capture areas from horizontal to 40 deg up for the hot nozzle ducts, and from 40 deg down to horizontal for the cold nozzle ducts. Since the flows sometimes impinged on either the top or the bottom walls of the ducts, the static pressure taps in those locations were used only to indicate flow direction. Taps in the sides of the ducts were used to determine static pressure for measurement of flow properties.

The method of measurement was as follows: Each total pressure finger on the rake was at the center of a rectangular section of flow area, which extended horizontally across the duct. The area was presumed to contain a two-dimensional, fully turbulent velocity distribution[4]; the flow properties were therefore integrated across each section from the pressure and temperature at the center, and the results added to get total flow properties.

The engine nozzle flows were then subtracted from the total mass flows calculated. The differences were the flows entrained into the ducts by the primary, or engine flows, whose stagnation properties were the cell ambient pressure and temperature. From the engine and entrained flow data, values were calculated for momentum and energy flow into the ducts.

Changes in total jet momentum, rather than total pressure, were used for the turning efficiency evaluations because, as the primary exhaust jet is turned, it spreads, and although the total pressure is reduced at the measuring station, it acts over a larger area. There is also some acceleration of the entrained flow, and some mixing of the two flows. The effect of the turning vanes and ducts on the redirected flow is friction drag and the production of secondary vortices and turbulence.

Samples of test data for momentum properties for the hot nozzle airflow are shown in Fig. 11.

Changes in kinetic energy plus flow work, rather than kinetic energy only, were used because of the changes in static pressure, and therefore in gas properties, from the duct inlets to the measuring stations. The energy losses come from frictional effects that convert kinetic energy and flow work into heat energy. Typical test data for the energy properties for the cold nozzle are shown in Fig. 12.

The flow properties for both engine and entrained flows were added together to get the total flow properties at the nozzle inlet. The results for flow properties at the inlets and the measuring stations were doubled to account for both sides of the engine, i.e., the measured and the unmeasured flows. Values of duct efficiency were calculated by dividing the measuring station momentum and energy by the corresponding inlet flow properties and expressing the results as percentages.

Summary

Overall performance parameters consisted of thrust measurements, jet turning efficiencies, and effect mechanisms associated with the installation. Installation results included the following:

1) Steady-state and transient engine testing was accomplished at various engine exhaust nozzle angles, from horizontal to vertical, at sea-level static conditions.

2) Jet momentum and energy losses were significant but not prohibitive; even at idle engine power, there was adequate momentum to remove the exhaust gases from the test cell.

3) Misalignments in incoming flow from the engine nozzles were easily tolerated by the vane cascades.

4) Flow entrained into the exhaust ducts by the nozzle jets was on the order of half the primary flow.

5) The slant thrust mode was the most severe for the thrust measuring system due to the overturning moment caused by the height of the engine above the thrust bed. Thrust measurements were within $\pm 3\%$ accuracy, compared to an accuracy of $\pm 1\%$ for the horizontal and vertical thrust modes.

6) Model test results with respect to cascade and exhaust duct geometry were verified; in particular, recirculation within the ducts was markedly reduced by designing the cascade to direct the exhaust toward a common capture area, rather than in a uniform direction.

7) There was no recirculation of exhaust gases back into the cell.

Conclusions

The following conclusions were drawn from the above program:

1) Compact installations can be built that will test high-thrust V/STOL engines, in vectored-thrust modes, in conventional enclosed test cells.

2) A vane cascade is a compact and efficient way to turn high-subsonic airflows, as well as incompressible flows, and can be used to advantage in the design of test installations for V/STOL propulsion systems.

3) The analysis used to determine flow properties in turning vane passages is effective for design work. In more rigorous investigations of cascade flows, it can also be used for initial estimates and modeling, into which real-fluid and secondary flow effects can subsequently be added.

Future Plans

Although the present program has resulted in the development of the only engine test chamber at any Navy facility with the capability to measure horizontal and vertical thrust of V/STOL engines, additional work is required before the full potential of the installation can be realized. The following tasks remain:

1) In order to improve the slant mode thrust measurement accuracy, a slight modification to the test stand design and/or readout equipment may be necessary.

2) The F402-RR-402 master correlation engine must be run in the chamber in both horizontal and vertical nozzle configurations to determine test cell correction factors.

Upon completion of these efforts, the test cell will be available for running aircraft mission profile tests that require the exhaust nozzles to be vectored from horizontal to vertical and vice versa. Examples of this type of testing are simulated mission endurance tests and also accelerated service tests for advanced AV-8 engines. More standardized engine tests requiring only horizontal or vertical thrust measurements can presently be conducted.

References

[1] *SAE Applied Thermodynamics Manual,* Society of Automotive Engineers, Inc., Committee A-9, Aerospace Environmental Systems, Feb. 1960, revised Jan. 1962.

[2] Shapiro, A.H., *The Dynamics and Thermodynamics of Compressible Flow,* Vol. I, The Ronald Press Co., New York, 1953.

[3] Kunz, K.S., *Numerical Analysis,* McGraw-Hill, New York, 1957.

[4] Schlichting, H., *Boundary Layer Theory,* 6th ed., McGraw-Hill, New York, 1968.